Electronic Supplementary Material (ESI) for Environmental Science: Processes & Impacts.
This journal is © The Royal Society of Chemistry 2015

ELETRONIC SUPPORTING INFORMATION

Physicochemical and ion-binding properties of highly aliphatic humic substances extracted from deep sedimentary groundwater

Takumi Saito*[a, b], Motoki Terashima[c], Noboru Aoyagi[d], Seiya Nagao[e], Nobuhide Fujitake[f], Toshihiko Ohnuki[b]

[a] Nuclear Professional School, School of Engineering, The University of Tokyo, 2-22 Shirakata Shirane, Tokai-mura, Ibaraki, 319-1188, Japan

[b] Advanced Science Research Center, Japan Atomic Energy Agency (JAEA), 2-4 Shirakata, Tokai-mura, Ibaraki, 319-1195, Japan

[c] Radioactive Waste Processing and Disposal Research Department, JAEA, 4-33 Muramatsu, Tokai-mura, Ibaraki, 319-1194, Japan

[d] Nuclear Science and Engineering Center, JAEA, 2-4 Shirakata, Tokai-mura, Ibaraki, 319-1195, Japan

[e] Institute of Natural and Environmental Technology, Kanazawa University, Wake, Nomi, Ishikawa 923-1224, Japan

[f] Graduate School of Agricultural Science, Kobe University, Rokkodai1, Kobe 657-8501, Japan

* Author to whom correspondence should be addressed. Phone: +81-29-284-3518; Fax: +81-29-282-5927; E-mail: saito.takumi@jaea.go.jp.

This supporting information contains 15 pages including 4 figures and 4 tables.

EAC determination by MER

The redox capacities of HHA, HFA and the standard and reference HSs from the IHSS and JHSS were indirectly determined by mediator electrochemical reduction (MER) as electron accepting capacities (EAC), according to Aeschbacher et al. [1,2]. Diquat dibromide monohydrate (DQ, 99.5%, Supelco) was used as a mediator. The electrochemical cell consisted of a reticulated vitreous carbon working electrode, a Pt auxiliary electrode, and a Ag/AgCl electrode with 3 M NaCl as the inner filling solution (BAS inc.). The auxiliary electrode was placed in a glass chamber separated from a test solution though a glass frit. The same buffer solution as used in the MER experiments was circulated though the chamber. Bulk electrolysis was performed with an ALS 600D potentiostat (BAS inc.) under moisturized Ar bubbling. The stock solutions of the HSs were made at 1 g/L in 0.1 M KCl (Wako Pure Chemical Industries) and 0.1 M K_2HPO_4/KH_2PO_4 (Wako Pure Chemical Industries) buffer at pH 7.0 and that of DQ was prepared at 5 mM in the same buffer medium.

Sixty milliliters of the buffer solution (0.1 M KCl and 0.1 M K_2HPO_4/KH_2PO_4) at pH 7.0 were first electrolyzed at -0.72 V (vs. Ag/AgCl) for at least 1 h. The voltage corresponds to -0.49 V (vs. SHE) and enough to reduce DQ, which was checked by cyclic voltammetry. After pre-electrolysis, 2 mL of the DQ solution was added, which was further electrolyzed for at least 1 h. Finally, 1 mL of a 1g/L HS solution was added to the solution. HS is rapidly reduced by DQ in the reduced form; oxidized DQ is then re-reduced on the surface of the electrode. EAC is calculated by integrating the reduction current upon this and normalized by the mass of the HS added to the cell.

NICA-Donnan modeling

In the NICA-Donnan model [3,4] the binding of an ion, *i*, to HS is described by

$$\begin{aligned} Q_i = {} & \frac{n_{1,j}}{n_{1,\mathrm{H}}} Q_{\max 1,\mathrm{H}} \frac{\left(\tilde{K}_{1,i} c_{\mathrm{D},i}\right)^{n_{1,i}}}{\sum_i \left(\tilde{K}_{1,i} c_{\mathrm{D},i}\right)^{n_{1,i}}} \frac{\left[\sum_i \left(\tilde{K}_{1,i} c_{\mathrm{D},i}\right)^{n_{1,i}}\right]^{p_1}}{1+\left[\sum_i \left(\tilde{K}_{1,i} c_{\mathrm{D},i}\right)^{n_{1,i}}\right]^{p_1}} \\ & + \frac{n_{2,j}}{n_{2,\mathrm{H}}} Q_{\max 2,\mathrm{H}} \frac{\left(\tilde{K}_{2,i} c_{\mathrm{D},i}\right)^{n_{2,i}}}{\sum_i \left(\tilde{K}_{2,i} c_{\mathrm{D},i}\right)^{n_{2,i}}} \frac{\left[\sum_i \left(\tilde{K}_{2,i} c_{\mathrm{D},i}\right)^{n_{2,i}}\right]^{p_2}}{1+\left[\sum_i \left(\tilde{K}_{2,i} c_{\mathrm{D},i}\right)^{n_{2,i}}\right]^{p_2}} \end{aligned}, \qquad \text{(S1)}$$

where the subscripts 1 and 2 denote low affinity sites and high-affinity sites, respectively, and $\tilde{K}_{j,i}$ and $n_{j,i}$ (j = 1 or 2) are the median value of the intrinsic affinity constant and the non-ideality parameter of an ion, *i*, for the site *j*, respectively. The parameters $Q_{\max j,\mathrm{H}}$ and p_j are the maximum density of proton binding sites and the heterogeneity parameter of the site *j*, respectively. Note that $n_{j,i}$ and p_j reflect the mean stoichiometry of the binding of the ion *i* to the site *j* ($n_{i,j}/n_{j,\mathrm{H}}$ = 1 for mono dentate binding and 0.5 for bi-dentate binding) and the width of the intrinsic affinity constant distribution (p_j = 1 for the homogeneous distribution) . Both $n_{j,i}$ and p_j span from 0 to 1. For H^+ binding without any other specifically binding metal ions eq. (S1) is simplified to a multi-site Langmuir-Freundlish equation:

$$Q_{\mathrm{H}} = Q_{\max 1,\mathrm{H}} \frac{\left(\tilde{K}_{1,\mathrm{H}} c_{\mathrm{H}}\right)^{m_1}}{1+\left(\tilde{K}_{1,\mathrm{H}} c_{\mathrm{H}}\right)^{m_1}} + Q_{\max 2,\mathrm{H}} \frac{\left(\tilde{K}_{2,\mathrm{H}} c_{\mathrm{H}}\right)^{m_2}}{1+\left(\tilde{K}_{2,\mathrm{H}} c_{\mathrm{H}}\right)^{m_2}}, \tag{S2}$$

where $m_j = n_{j,i} \times p_j$. The charge of HS is then calculated as $Q_{\mathrm{H}} - (Q_{\max 1,\mathrm{H}} + Q_{\max 2,\mathrm{H}})$, which relates to the experimentally determined charge, *q*, by potentiometric titration via

$$q + q_0 = Q_{\mathrm{H}} - (Q_{\max 1,\mathrm{H}} + Q_{\max 2,\mathrm{H}}). \tag{S3}$$

In this equation q_0 is the initial charge of the HS at the beginning of the titration and is usually unknown beforehand and treated as an adjustable parameter, unless one has prior knowledge on the amounts of free acid or other H^+-consuming impurities in the sample.[3]

The concentration of the ion *i* in the vicinity of the HS binding sites are expressed as $c_{\mathrm{D},i}$, which relates to the bulk concentration, c_i^0, by the Boltzmann factor with the Donnan potential, ψ_{D}:

$$c_{\mathrm{D},i} = c_i^0 \exp\left(-\frac{z_i e \psi_{\mathrm{D}}}{k_{\mathrm{B}} T}\right), \tag{S4}$$

where z_i is the valence of ion *i*, *e* the elementary charge, k_{B} the Boltzmann constant and *T* the absolute temperature. In the Donnan model the negative charge of HS is neutralized inside the so-called Donnan volume, V_{D} (L/Kg), which is approximated by a function of the ionic strength of the solution, *I,* with an adjustable Donnan parameter, *b*:

$$\log V_{\mathrm{D}} = -1 + b(1 - \log I) \tag{S5}$$

The measured H^+ and Cu^{2+} binding isotherms to HHA and HFA were fitted to the NICA-Donnan model, using an in-house MATLAB® program and following the procedure proposed by Kinniburgh et al.[3] First, $Q_{\max j,\mathrm{H}}$, $\tilde{K}_{j,\mathrm{H}}$, m_j, *b*, and q_0 were optimized by fitting eq. (S2) to the charge/pH curves of the HHSs. Then, $\tilde{K}_{j,\mathrm{Cu}}$, $n_{j,\mathrm{H}}$, $n_{j,\mathrm{Cu}}$, and p_j were optimized by fitting eq. (S1) to the Cu^{2+} binding isotherms to the HHSs, while m_j was kept to the values determined in the previous step. For $n_{j,i}$ and p_j, the lower and upper boundaries were set to 0 and 1, respectively.

XAS data reduction and theoretical fitting

The Cu K-edge XAS spectra were processed using the Athena program.[5] For edge-step normalization and conversion into k-space, the energy of edge of the Cu K-edge (8.992 keV) was defined as the first inflection point of the edge. Background correction was performed by subtracting a first-order polynomial fit to the pre-edge region (−150 to −40 eV) and by a third-order polynomial fit to the post-edge region (170 to 590 eV). The EXAFS oscillation was extracted by subtracting a fit to a piece-wise spline function using the Autobk algorithm with Rbkg = 1.1, *k* weight = 3, and *k* range = 0.5 - 12.5 Å^{-1}. The k^3-weighted EXAFS spectra from 2.4 to 11.6 Å^{-1} was Fourier-transformed using the Hanning window with d*k* = 2.

The first coordination sphere of Cu^{2+} bound to the HA was modeled by theoretical fitting using the Artemis program [5] and the *ab initio* program FEFF6 for theoretical scattering phases and amplitude functions.[6] Diauabis ethylthioacetato copper was used as a model compound for the FEFF6.[7] Due to relatively large abundance of S, the first shell of Cu^{2+} bound to HHA was modeled by two scatter elements, O/N and S; whereas that to PAHA was modeled by single O/N scatter. The amplitude reduction factor (S_0^2) optimized for the modeling of the first coordination shell of the reference Cu^{2+}-tartrate complex ($S_0^2 = 0.95$) was used throughout the fitting. In order to reduce the number of adjustable parameters and obtain reasonable values, the Debye-Waller factor of the Cu-S shell was set to be equal to that of the Cu-O/N shell.

Table S1 Physicochemical properties of the HHSs, the IHSS and JHSS reference HSs, and PAHA.

Name [a]	Origin	Elemental composition (%)						^{13}C-NMR Carbon distribution				
		C	N	N	O	S	Ash	C_I	C_{II}	C_{III}	$C_{IV} + C_V$	Aromaticity
Horonobe HSs												
HHA	Groundwater	62.3	6.4	3.4	25.4	2.5	N.D.	3	13	26	59	0.31
HFA	Groundwater	60.2	6.8	2.1	29.0	1.9	N.D.	4	14	21	61	0.26
IHSS, JHSS, and commercial HAs												
EHA	Soil	58.1	3.7	4.1	34.1	0.4	1	6	18	50	26	0.66
IHA	Soil	54.8	4.3	4.0	36.6	0.3	1	1	17	48	34	0.59
DHA	Soil	53.0	5.3	4.5	36.9	0.3	1	2	17	29	52	0.36
PHA	Peat	56.4	3.8	3.7	37.3	0.7	1	5	20	47	28	0.63
PAHA	Commercial	55.8	4.6	0.6	38.9	-	1	4	16	56	24	0.70
LHA	Lignin	63.8	3.7	1.2	31.3	0.8	3	8	15	58	19	0.75
SRHA	River	52.6	4.3	1.2	42.0	0.5	1	6	15	31	49	0.39
NHA	Lake	53.3	4.0	1.2	43.1	0.6	0	10	19	38	33	0.54
IHSS and JHSS FAs												
IFA	Soil	43.3	3.5	1.7	51.4	0.1	6	3	23	30	44	0.41
DFA	Soil	47.6	3.5	0.8	48.1	0.0	2	4	24	30	42	0.42
BFA	Lake	56.1	6.1	2.3	35.5	-	2	6	14	17	63	0.21
NFA	Lake	52.3	4.0	0.7	45.1	0.5	1	10	24	31	37	0.46
SRFA	River	52.3	4.4	0.7	43.0	0.5	1	5	17	22	57	0.28

a. The elemental compositions are weight % on ash and water-free basis, taken from http://www.ihss.gatech.edu/elements.html for the IHSS samples, Watanabe et al. [8] for the JHSS samples, Vermeer et al. [9] for PAHA, and Terashima et al. [10] for the HHSs samples.

b. C_I = carbonyl (190 - 220 ppm), C_{II} = carboxyl (165 - 190 ppm), C_{III} = aromatic (110 - 165 ppm), C_{IV} = methoxyl and carbohydrate (48 - 110 ppm), CV = aliphatic carbon (5-48 ppm). For the sake of comparision the sums of C_{IV} and C_V are shown. Aromaticity is defined as $C_{III}/(C_{IV} + C_V)$. The values were taken from http://www.ihss.gatech.edu/thornnmr.html for the IHSS samples, Watanabe et al. [8] for the JHSS samples, Vermeer et al. [9] for PAHA, and Terashima et al. for the HHSs samples.

Table S1 Continued.

Name	UV/Vis absorption [c]			Acidic functional groups (meq/g)[d]				Peak size[e] (nm)
	$A_{400/600}$	$A_{250/210}$	A_{350}/A_{280}	q_1	q_2	q_3	$q_1/(q_1+q_2)$	
Horonobe HSs								
HHA	21.02	0.48	0.33	6.9	0.7	3.9	0.60	0.55
HFA	13.87	0.33	0.29	9.8	1.1	2.4	0.74	0.30
IHSS, JHSS, and commercial HAs								
EHA	6.53	0.82	0.56	8.3	1.9	5.1	0.54	2.49
IHA	6.96	0.82	0.54	7.7	3.5	5.2	0.47	1.94
DHA	7.68	0.66	0.45	8.1	3.2	6.1	0.47	2.00
PHA	8.38	0.77	0.50	9.0	1.9	4.7	0.58	2.06
PAHA	9.38	0.83	0.54	8.0	3.8	0.8	0.64	2.25
LHA	7.97	0.84	0.53	7.5	2.3	1.4	0.67	2.43
SRHA	25.23	0.63	0.41	9.1	3.7	1.6	0.63	2.37
NHA	15.61	0.63	0.47	9.1	3.2	1.6	0.65	2.06
IHSS and JHSS FAs								
IFA	34.09	0.65	0.29	12.4	1.6	2.9	0.74	0.84
DFA	25.82	0.67	0.35	11.7	2.2	1.2	0.78	0.90
BFA	26.54	0.55	0.31	9.1	1.7	2.9	0.66	0.87
NFA	23.83	0.64	0.43	11.2	3.2	0.9	0.70	1.75
SRFA	16.33	0.68	0.48	11.2	2.8	0.9	0.75	1.50

c. The absorbance at 280 nm (A_{280}) as well the absorbance ratios at 400 and 600 nm ($A_{400/600}$), 250 and 210 nm ($A_{250/210}$), and 350 and 280 nm ($A_{350/280}$) are shown. The values were determined in this study.

d. The concentrations of the carboxylic (q_1) and phenolic (q_2) groups were determined from potentiometric titration with following definitions: q_1 was the charge density (meq/g C) at pH 8.0; and q_2 was two times the change in the charge density between pH 8.0 and pH 10.0. The concentrations of nitrogen-bearing functional groups (q_3) were converted from the elemental composition of nitrogen in % (w/w). The values of HHA and HFA were determined in this study and those of the IHSS standards are taken from http://www.ihss.gatech.edu/elements.html and those of the JHSS standards and PAHA from Luckman et al.[11]

e. Determined as the size at the maximum UV/Vis absorbance in the fractograms obtained by Fl-FFF (see the main text). The values are taken from Luckman et al.[11], except for those of HHA and HFA, which were determined in this study.

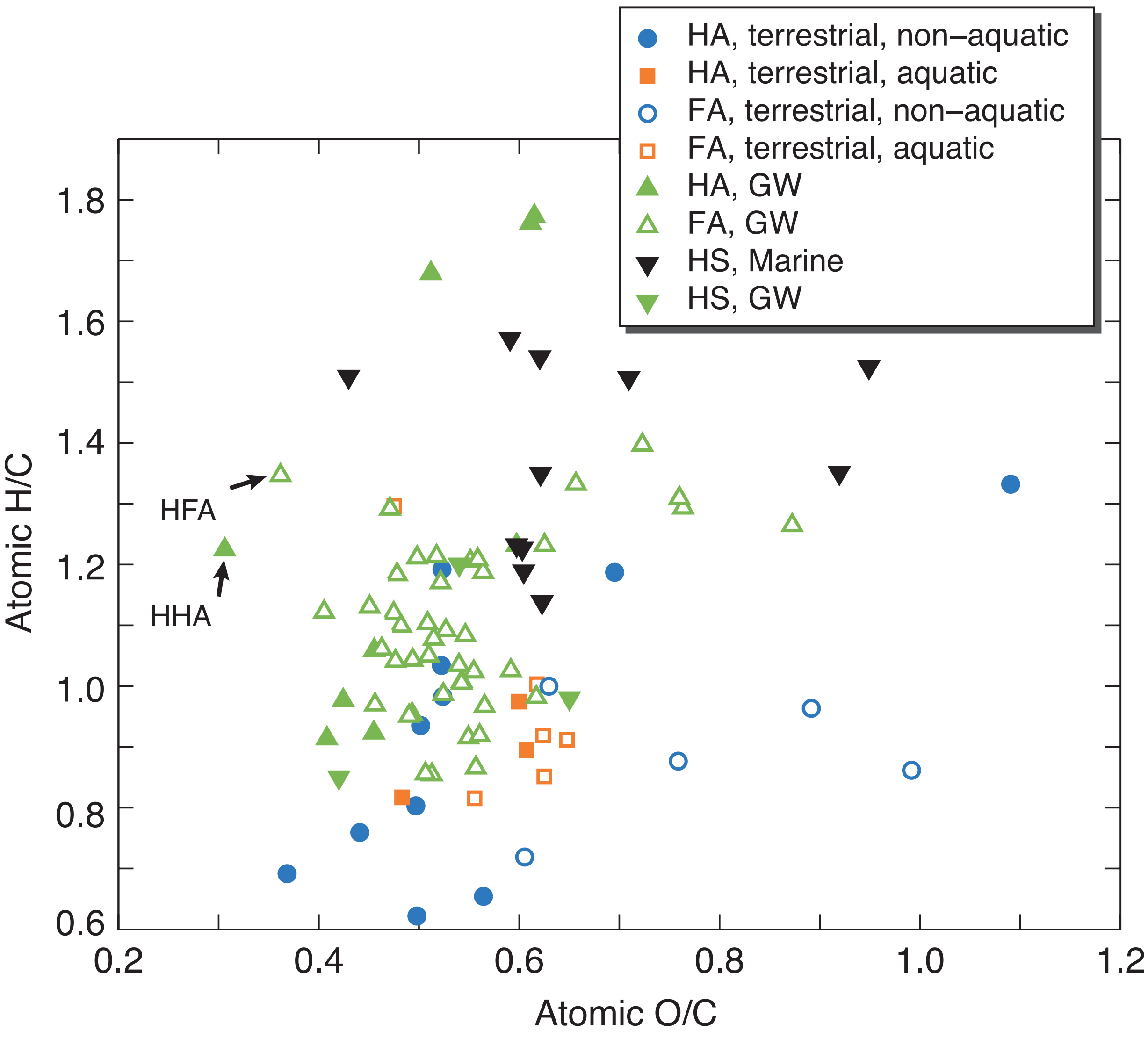

Fig. S1 van Krevelen plot of HHA and HFA together with HAs and FAs from various origins.[8, 9, 11-17]

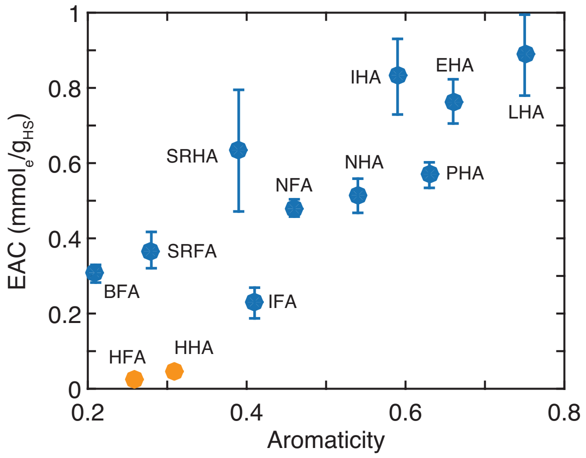

Fig. S2 Electron accepting capacities of the HHS and the IHSS and JHSS standard and reference HSs determined by mediator electrochemical reduction with diquat.

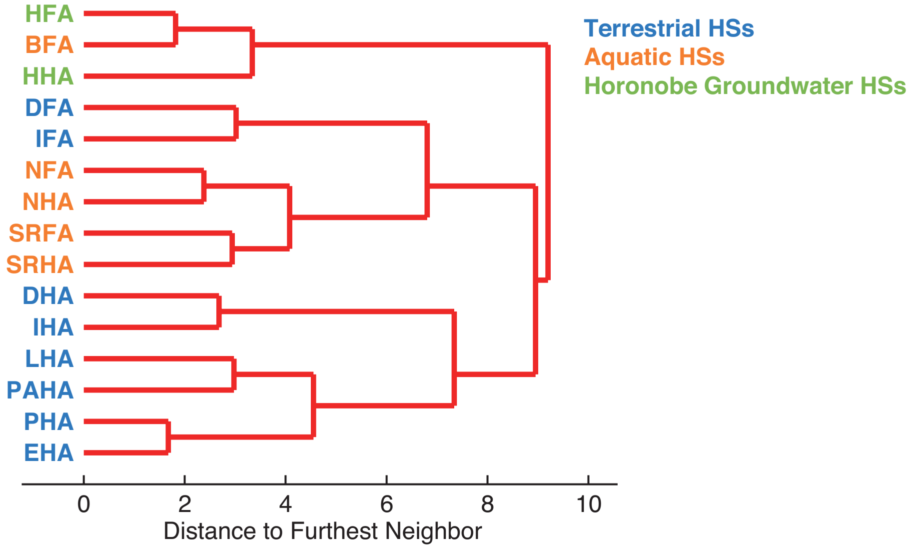

Fig. S3 Dendrogram of the cluster analysis of the physicochemical properties of HHSs, IHSS and JHSS reference HSs, and PAHA in Table S1. Clusters of the items are formed on the basis of distance to furthest neighbor.

Table S2 Optimized NICA-Donnan parameters for H^+ and Cu^{2+} binding to HHA and HFA with the 95% confidence intervals.

	HHA	HFA
q_0 (eq/Kg)	-0.64 (0.18)	-0.53 (0.23)
b	0.81 (0.05)	0.87 (0.05)
$Q_{\mathrm{max1,\,H}}$ (eq/Kg)	4.38 (0.36)	5.64 (0.96)
p_1	*1*[a] (0.17)	*1*[a] (0.41)
$Q_{\mathrm{max2,\,H}}$ (eq/Kg)	4.44 (11.13)	4.09 (42.90)
p_2	0.36 (0.25)	0.27 (1.07)
$\log \tilde{K}_{1,\mathrm{H}}$	3.74 (0.12)	3.63 (0.12)
$n_{1,\,\mathrm{H}}$	0.82 (0.12)	*1*[a] (0.42)
$\log \tilde{K}_{2,\mathrm{H}}$	10.62 (4.56)	10.48 (26.23)
$n_{2,\,\mathrm{H}}$	*1*[a] (0.31)	*1*[a] (2.10)
$\log \tilde{K}_{1,\mathrm{Cu}}$	1.32 (0.24)	1.16 (0.38)
$n_{1,\,\mathrm{Cu}}$	*1*[a] (0.08)	*1*[a] (0.19)
$\log \tilde{K}_{2,\mathrm{Cu}}$	14.43 (12.65)	15.05 (145.60)
$n_{2,\,\mathrm{Cu}}$	0.28 (0.09)	0.29 (2.33)

a. The values in italic are constrained in physically meaningful ranges of the corresponding parameters.

Table S3. Correlation matrix of the optimized NICA-Donnan parameters for HHA.

	$Q_{\mathrm{max1,\,H}}$	$Q_{\mathrm{max2,\,H}}$	$\log\tilde{K}_{1,\mathrm{H}}$	$\log\tilde{K}_{2,\mathrm{H}}$	$\log\tilde{K}_{1,\mathrm{Cu}}$	$\log\tilde{K}_{2,\mathrm{Cu}}$	$n_{1,\,\mathrm{H}}$	$n_{2,\,\mathrm{H}}$	$n_{1,\,\mathrm{Cu}}$	$n_{2,\,\mathrm{Cu}}$	p_1	p_2	b	q_0
$Q_{\mathrm{max1,\,H}}$	1.000	-0.271	0.054	-0.372	-0.432	-0.379	-0.326	0.123	-0.082	0.145	-0.604	0.742	0.390	-0.829
$Q_{\mathrm{max2,\,H}}$		1.000	0.011	0.983	0.130	0.904	0.016	-0.526	0.075	-0.775	0.139	-0.448	0.036	0.084
$\log\tilde{K}_{1,\mathrm{H}}$			1.000	-0.010	0.671	-0.030	-0.484	0.005	-0.007	0.027	0.297	0.199	0.691	0.227
$\log\tilde{K}_{2,\mathrm{H}}$				1.000	0.173	0.933	0.067	-0.511	0.076	-0.758	0.167	-0.578	0.024	0.127
$\log\tilde{K}_{1,\mathrm{Cu}}$					1.000	0.157	-0.066	-0.097	0.386	-0.086	0.406	-0.234	0.458	0.455
$\log\tilde{K}_{2,\mathrm{Cu}}$						1.000	0.257	-0.200	-0.121	-0.794	0.018	-0.706	0.019	0.121
$n_{1,\,\mathrm{H}}$							1.000	0.388	-0.303	-0.127	-0.475	-0.508	-0.309	0.073
$n_{2,\,\mathrm{H}}$								1.000	-0.551	0.403	-0.380	-0.104	0.014	-0.046
$n_{1,\,\mathrm{Cu}}$									1.000	-0.036	0.313	0.166	-0.071	0.088
$n_{2,\,\mathrm{Cu}}$										1.000	0.053	0.320	-0.031	0.007
p_1											1.000	-0.139	-0.201	0.728
p_2												1.000	0.179	-0.356
b													1.000	-0.409
q_0														1.000

Table S4. Correlation matrix of the optimized NICA-Donnan parameters for HFA.

	$Q_{\mathrm{max1,\,H}}$	$Q_{\mathrm{max2,\,H}}$	$\log \tilde{K}_{1,\mathrm{H}}$	$\log \tilde{K}_{2,\mathrm{H}}$	$\log \tilde{K}_{1,\mathrm{Cu}}$	$\log \tilde{K}_{2,\mathrm{Cu}}$	$n_{1,\,\mathrm{H}}$	$n_{2,\,\mathrm{H}}$	$n_{1,\,\mathrm{Cu}}$	$n_{2,\,\mathrm{Cu}}$	p_1	p_2	b	q_0
$Q_{\mathrm{max1,\,H}}$	1.000	-0.866	-0.044	-0.870	-0.461	-0.422	-0.322	0.023	0.008	-0.011	-0.141	0.774	0.081	-0.213
$Q_{\mathrm{max2,\,H}}$		1.000	-0.003	1.000	0.341	0.497	0.281	-0.014	-0.019	-0.002	0.040	-0.830	0.057	-0.173
$\log \tilde{K}_{1,\mathrm{H}}$			1.000	0.000	0.533	0.006	-0.137	-0.006	-0.032	-0.013	0.150	0.020	0.737	0.363
$\log \tilde{K}_{2,\mathrm{H}}$				1.000	0.345	0.497	0.282	-0.014	-0.019	-0.002	0.041	-0.833	0.062	-0.173
$\log \tilde{K}_{1,\mathrm{Cu}}$					1.000	0.464	0.521	-0.010	0.092	-0.447	-0.306	-0.309	0.381	0.292
$\log \tilde{K}_{2,\mathrm{Cu}}$						1.000	0.768	0.684	-0.613	-0.837	-0.633	-0.784	0.039	-0.099
$n_{1,\,\mathrm{H}}$							1.000	0.369	-0.482	-0.794	-0.863	-0.458	-0.111	0.002
$n_{2,\,\mathrm{H}}$								1.000	-0.834	-0.605	-0.392	-0.525	0.000	-0.016
$n_{1,\,\mathrm{Cu}}$									1.000	0.553	0.495	0.463	-0.039	0.015
$n_{2,\,\mathrm{Cu}}$										1.000	0.825	0.325	-0.014	0.013
p_1											1.000	0.165	-0.035	0.266
p_2												1.000	-0.028	0.115
b													1.000	-0.276
q_0														1.000

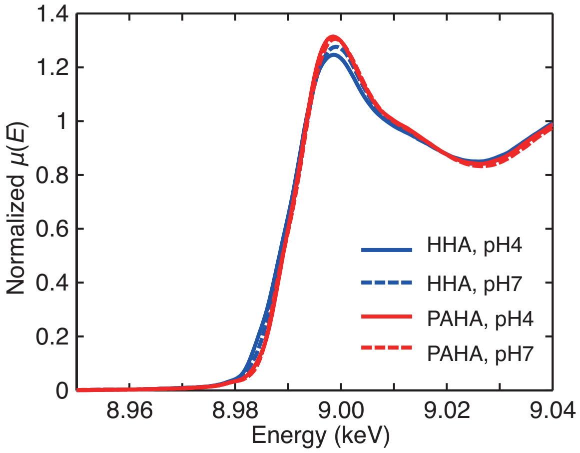

Fig. S4 Magnified and overlapped XANES spectra of Cu^{2+} bound to HHA and PAHA at pH 4 and 7.

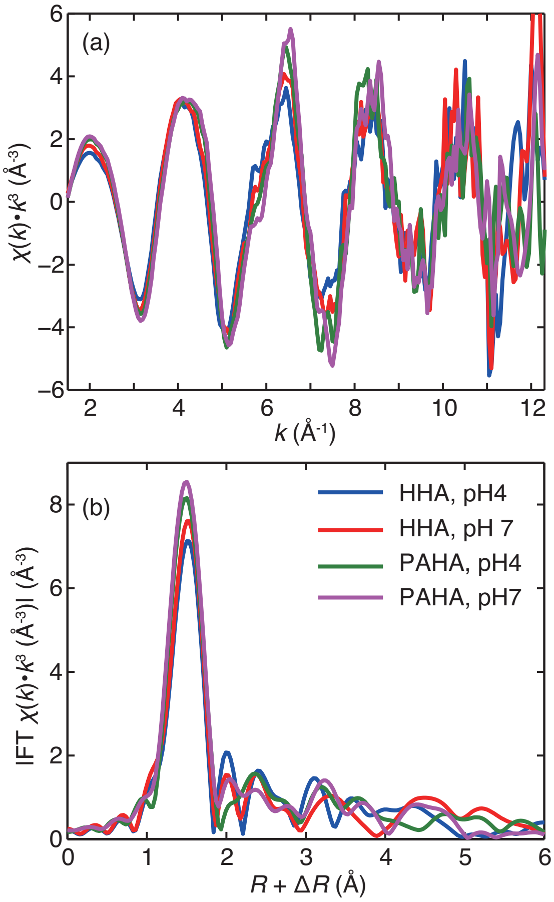

Fig. S5 Overlapped plots of the k^3-weighted Cu K-edge EXAFS spectra (a) and the corresponding Fourier transform magnitude (b) of Cu^{2+} bound to HHA and PAHA at pH 4 and 7 in Fig. 5.

References in SI

1. M. Aeschbacher, D. Vergari, R. P. Schwarzenbach and M. Sander, *Environ. Sci. Technol.*, 2011, **45**, 8385-8394.
2. M. Aeschbacher, M. Sander and R. P. Schwarzenbach, *Environ. Sci. Technol.*, 2010, **44**, 87-93.
3. D. G. Kinniburgh, W. H. van Riemsdijk, L. K. Koopal, M. Borkovec, M. F. Benedetti and M. J. Avena, *Colloids Surf. A*, 1999, **151**, 147-166.
4. L. K. Koopal, T. Saito, J. P. Pinheiro and W. H. van Riemsdijk, *Colloids Surf. A*, 2005, **265**, 40-54.
5. B. Ravel and M. Newville, *J. Synchrotron Rad.*, 2005, **12**, 537-541.
6. S. I. Zabinsky, J. J. Rehr, A. Ankudinov, R. C. Albers and M. J. Eller, *Phys. Rev. B*, 1995, **52**, 2995-3009.
7. T. Ogawa, M. Shimoi and A. Ouchi, *Bull. Chem. Soc. Jpn.*, 1982, **55**, 126-129.
8. A. Watanabe, K. Itoh, S. Arai and S. Kuwatsuka, *Soil Science Plant Nutrition*, 1994, **40**, 601-608.
9. A. W. P. Vermeer, W. H. van Riemsdijk and L. K. Koopal, *Langmuir*, 1998, **14**, 2810-2819.
10. M. Terashima, K. Iijima, S. Nagao, N. Fujitake, M. Okazaki and Y. Tachi, *Submitted*, 2015.
11. S. Lukman, T. Saito, N. Aoyagi, T. Kimura and S. Nagasaki, *Geochim. Cosmochim. Acta*, 2012, **88**, 199-215.
12. C. Pettersson, J. Ephraim and B. Allard, *Org. Geochem.*, 1994, **21**, 443-451.
13. S. Nagao, T. Iwatsuki and K. Hama, *J. Nucl. Fuel Cycle Environ.*, 2009, **15**, 77-86 (in Japanese).
14. C. Gron, L. Wassenaar and M. Krog, *Environ. Int.*, 1996, **22**, 519-534.
15. T. D. Gauthier, W. R. Seitz and C. L. Grant, *Environ. Sci. Technol.*, 1987, **21**, 243-248.
16. R. Artinger, G. Buckau, S. Geyer, P. Fritz, M. Wolf and J. I. Kim, *Appl. Geochem.*, 2000, **15**, 97-116.
17. J. J. Alberts, Z. Filip and N. Hertkorn, *J. Contam. Hydrol.*, 1992, **11**, 317-330.